Vacuum-Free, Maskless Patterning of Ni Electrodes by Laser Reductive Sintering of NiO Nanoparticle Ink and Its Application to Transparent Conductors

Daeho Lee,[‡,*] Dongwoo Paeng,[†] Hee K. Park,[§] and Costas P. Grigoropoulos[†,*]

[†]Laser Thermal Laboratory, Department of Mechanical Engineering, University of California, Berkeley, California 94720-1740, United States, [‡]Department of Mechanical Engineering, Gachon University, Seongnam-si, Gyeonggi-do 461-701, South Korea, and [§]Laser Prismatics LLC, San Jose, California 95129, United States

ABSTRACT We introduce a method for direct patterning of Ni electrodes through selective laser direct writing (LDW) of NiO nanoparticle (NP) ink. High-resolution Ni patterns are generated from NiO NP thin films by a vacuum-free, lithography-free, and solution-processable route. In particular, a continuous wave laser is used for the LDW reductive sintering of the metal oxide under ambient conditions with the aid of reducing agents in the ink solvent. Thin (~40 nm) Ni electrodes of glossy metallic surfaces with smooth morphology and excellent edge definition can be fabricated. By applying this method, we demonstrate a high transmittance (>87%), electrically conducting panel for a touch screen panel application. The resistivity of the Ni electrode is less than an order of magnitude higher compared to that of the bulk Ni. Mechanical bending test, tape-pull test, and ultrasonic bath test confirm the robust adhesion of the electrodes on glass and polymer substrates.

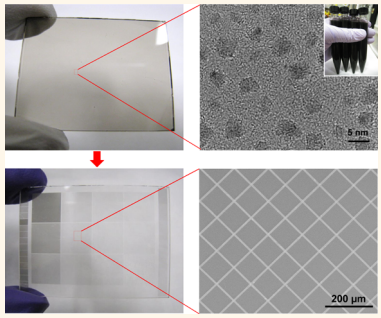

KEYWORDS: selective laser reductive sintering · Ni electrode · solution-processable route · NiO nanoparticle ink · touch screen panel · flexible substrate

Recently, photolithography-free electrode fabrication methods have garnered substantial attention due to the increasing demand for flexible electronics and low-cost fabrication routes. Screen printing[1,2] and inkjet printing[3−5] are well-known deposition methods for these purposes and are commonly employed for solar cell and screen panel manufacturing, although they have limitations with respect to high-resolution patterning. In this context, a laser direct writing (LDW) process[6−9] offers a promising route. Nonvacuum solution-processable thin film deposition methods utilizing nanoparticle (NP) inks[7,10,11] enable low-temperature treatment by taking advantage of the significant depression of the NP melting point with reduced size. Consequently, the combination of NP ink deposition and LDW can effectively perform high-resolution, direct patterning of electrodes on various types of substrates without inflicting thermal damage.[11−14] Most of the target materials for metal electrodes have been noble metals such as silver[11,13,14] and gold[15,16] due to their resistance to oxidation, even in NP configurations. The biggest challenge in utilizing inexpensive metals such as copper (Cu), aluminum (Al), and nickel (Ni) is that they are easily oxidized in air due to the low oxidation potential. Moreover, oxidation accelerates as the surface area increases and is therefore more pronounced for small-sized particles. For this reason, synthesizing NPs of common metals such as Cu, Al, and Ni usually requires an inert environment, increasing the facility complexity and eventually the material cost. Furthermore, such NPs are easily oxidized during storage, handling, and post-processing performed under ambient conditions.

Recently, several researchers have attempted to fabricate metal electrodes by reduction of metal oxide. For example, copper electrodes, as alternatives to noble metals, were fabricated by local reduction of

* Address correspondence to cgrigoro@berkeley.edu, dhl@gachon.ac.kr.

Received for review June 23, 2014 and accepted August 17, 2014.

Published online August 17, 2014
10.1021/nn503383z

copper(I or II) oxide (Cu_2O or CuO) NPs using pulsed laser[17,18] or intense pulsed light.[19,20] Through localized reductive sintering of copper oxide NPs, highly conductive copper electrodes were successfully generated. However, the feature resolution of electrodes fabricated through these methods is limited due to the relatively large (>30 nm) and uneven size of the CuO NPs. Copper is also susceptible to oxidation at the working temperature of electronics, which causes degradation of its electrical properties.

Ni, in contrast to Cu, is known to be corrosion-resistant and hence is commonly used as a component of alloys and a plating material. For this reason, Ni is also widely used as current collector in energy storage devices such as super capacitors and batteries. Ni films have been deposited by several ways including electrodeposition,[21] sputtering,[22] pulsed laser deposition,[23] atomic layer deposition,[24] and chemical bath deposition.[25] Electron-beam-based deposition is not appropriate for Ni due to its ferromagnetic nature.[26] As an alternative method, Ni electrodes generated by flash light sintering of Ni NPs have been reported.[27] Flash light irradiation effectively sintered varying diameter (5−500 nm) Ni NPs to yield highly conductive electrodes.

In this paper, we introduce high-resolution direct patterning of Ni electrodes through reductive sintering of a solution-processed NiO thin film by the LDW process and its application for a transparent touch screen panel. Here, the term "reductive sintering" refers to the phenomenon wherein reduction occurs just before the sintering process. Through this method, high-resolution Ni patterns are generated from NiO NP thin films by a vacuum-free, lithography-free, and solution-processable route. The transmittance and conductance of the fabricated thin electrodes are high enough to be applied to the transparent touch screen panels. The continuous wave (CW) laser reductive sintering can also generate Ni patterns on a plastic substrate due to the minimized thermal effect on the substrate during laser processing.

RESULTS AND DISCUSSION

The NiO NPs were synthesized on the basis of a previously reported method[28] with several modifications. The details of the synthesis procedures are described in the Materials and Methods section. The fabrication procedure referred to aims at synthesizing Ni catalysts and should be performed under nitrogen flow to prevent oxidation of the NPs. However, the NiO NP synthesis process developed in this study does not require an inert environment. Thus, the entire process flow from the materials synthesis to the laser process for Ni electrode fabrication in this study is conducted under ambient conditions.

The size of synthesized NiO NPs is 2−3 nm with uniform distribution as verified by TEM (Figure 1a). The synthesized NPs can be well-dispersed in various solvents, including toluene (C_7H_8) and α-terpineol ($C_{10}H_{18}O$) without agglomeration (Figure 1a inset), so that high-quality thin films can be deposited by spin-coating on an oxygen-plasma-treated soda-lime glass substrate as demonstrated in the optical microscope and SEM (scanning electron microscope) images (Figure 1b,c). It is also possible to deposit NiO thin films by dip-coating or inkjet printing of the NiO NP ink. The NP concentration and solid content in the ink are easily adjustable. Varying the ink concentration or the spin-coating process parameters can control the thin film thickness. In this study, the concentration of the NiO NP in the ink and the spin speed are fixed at 1.1% by weight and 2000 rpm, respectively, to produce uniform 230 nm thick NiO films. The lifetime limit of the NiO ink is not fully tested yet, although it is stable over at least 2 weeks.

The prepared film is processed by LDW to incur reductive sintering. A 514.5 nm CW laser beam is employed with a Gaussian beam profile of 4.6 μm ($1/e^2$) diameter obtained through a 10× infinity-corrected objective lens. Since the absorption of the NiO film extends over a wide range, the processing can be done by using lasers at other wavelengths, such as in the ultraviolet (UV) and visible (vis) ranges. Figure 1d shows the schematic illustration of the LDW setup. The laser power is adjusted to produce reductively sintered electrodes at a fixed scanning speed of 10 mm/s. The optimum laser power depends on the substrate type. After the LDW, the unsintered parts of the thin film are washed away with the same solvent as in the ink, whereas the sintered parts adhere to the substrate. Figure 1e shows mesh-type Ni electrode patterns defined on a glass substrate by laser beam scanning in two orthogonal directions. After laser irradiation, the irradiated part of the NiO film turns into a shiny Ni electrode. The inset of Figure 1e shows glossy surfaces of the plane-type Ni electrode under illumination, confirming specular reflection due to the smooth and uniform surface topography. LDW also enables one-step arbitrary patterning linked with a CAD (computer-aided design) system (Figure 1f).

Figure 2a shows a scanning electron microscopy (SEM) image of an electrode line defined by a single scan of the laser beam at a power of around 159 kW/cm^2. The line width of the electrode is measured to be approximately 6.5 μm, which is related to temperature distribution induced by the laser irradiation. The maximum temperature increases at higher laser power and slower scan speed, hence enlarging the electrode width.[13] Figure 2b, c shows top view SEM images of the mesh-type electrodes with different magnifications. It is worth noting that the edges of the laser-sintered electrode lines are sharp, suggesting that this LDW reductive sintering process can be applied to a high-resolution electrode fabrication.

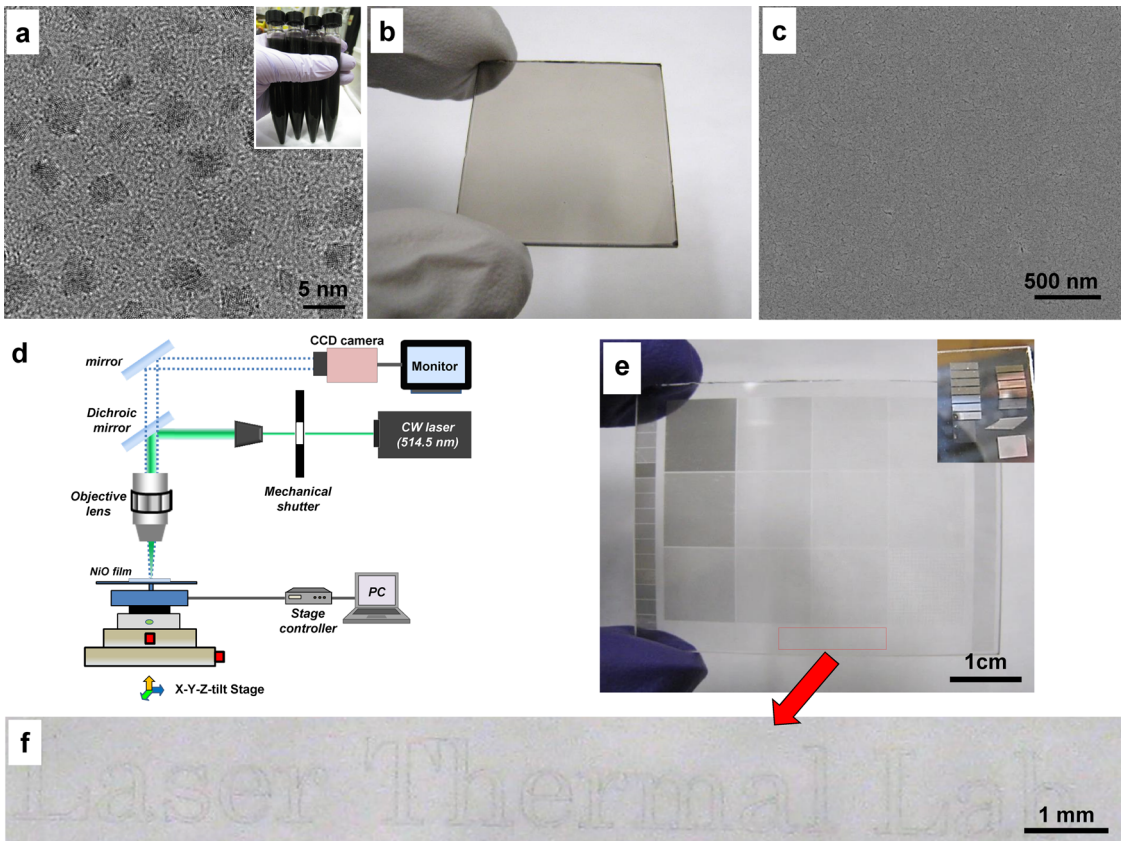

Figure 1. (a) TEM image of synthesized NiO nanoparticles. (b) Spin-coated NiO thin film on a glass substrate. (c) SEM image of the surface of the NiO film shown in (b). (d) Schematic illustration of the laser direct writing setup. (e) Mesh-type Ni electrodes defined by laser reductive sintering of the NiO thin film. Each area is produced by mesh patterns of different pitches. The inset is a photograph of glossy surfaces of plane-type Ni electrodes under natural illumination. (f) Arbitrary patterns (letters) on a glass substrate generated by laser direct writing process linked with a CAD system.

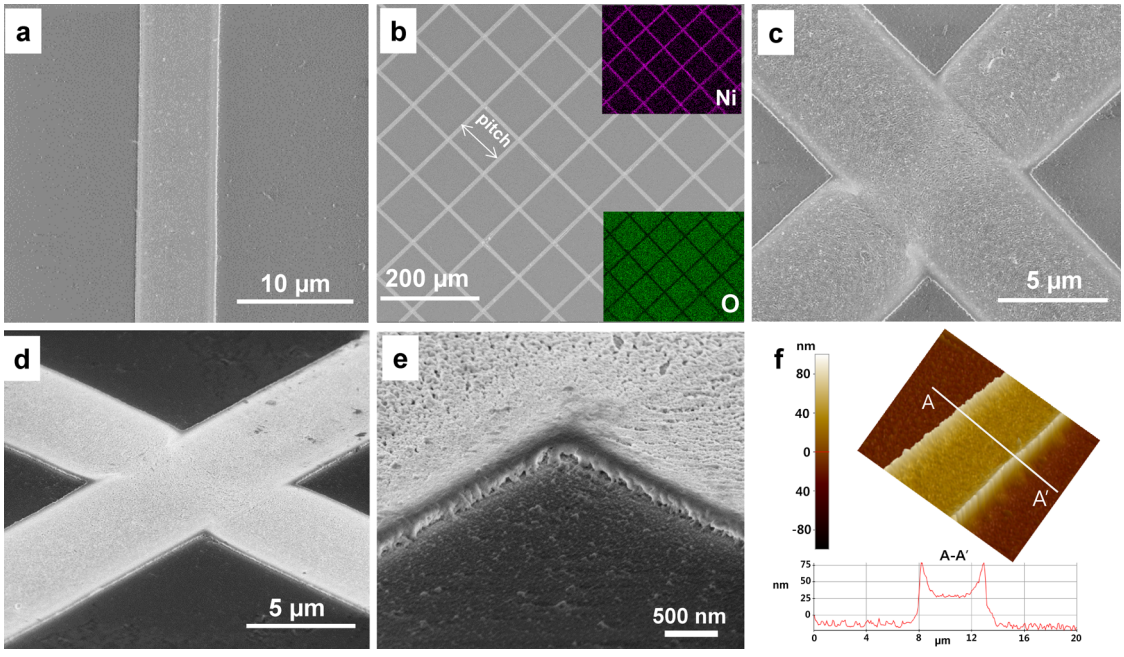

Figure 2. (a) Top view SEM image of a single Ni electrode. The line width is around 6.5 μm. (b,c) Top view SEM images of mesh-type electrodes with different magnifications. The mesh-type Ni grids are generated by two-time laser scanning—one time per each direction. (d,e) Tilted view images of the intersection area of the mesh patterns. (f) AFM image of a single electrode. The cross-sectional shape is plotted on different axis scales.

Insets in Figure 2b are the elemental mapping images for Ni and O acquired from energy-dispersive X-ray spectroscopy (EDX) analysis of the mesh-type electrodes on a glass substrate. EDX analysis was carried out at an accelerating voltage of 2 keV. The images show a clear contrast between Ni and O elements in the electrodes, suggesting that laser irradiation effectively removes oxygen from the NiO NP film while the washing process cleanly removes the nonirradiated parts. The tilted view images of the intersection area of the mesh patterns in Figure 2d,e further show the feature quality. The electrode is thicker near the edge than at the center due to thermocapillarity,[16] and the nominal thickness of the electrode measured by atomic force microscopy (AFM) is around 35−40 nm, as shown in Figure 2f. The rms (root mean square) value of the surface roughness at the center area of the electrode is around 2.6 nm. It is noted that the contrast of the thickness in the cross-sectional shape is amplified by the different axis scales (*x*-axis, μm; *y*-axis, nm). We expect that a flatter shape of the electrodes can be achieved by employing a top-hat laser beam or the two-beam configuration,[16] which reduces the temperature gradient on the laser-irradiated area.

The reduction mechanism of the NiO thin film induced by laser irradiation is not completely understood yet but can be inferred from reported studies on the reduction of copper oxide thin films. For example, the reduction of a CuO thin film deposited with ethylene glycol ($C_2H_6O_2$)-based CuO NP ink was attributed to a photochemical reaction of CuO NPs with ethylene glycol at an elevated temperature.[17] On the other hand, the reduction of PVP (polyvinylpyrrolidone)-retained CuO NPs under intense pulsed light was ascribed to the hydroxyl (−OH) end group of PVP which acts like a long-chain alcohol and serves as a reducing agent.[19] Prior to these studies, a more general mechanism was suggested for Cu_2O reduction with the aid of alcohols, aldehydes, or carboxylic acid as reducing agents.[29] It is also known that metal oxide can be reduced at a high temperature with forming gas ($N_2 + H_2$) or natural gas (mainly methane), which can be described by the following simple reactions, $CuO(s) + H_2(g) \rightarrow Cu(s) + H_2O(g)$ or $4CuO(s) + CH_4(g) \rightarrow 4Cu(s) + 2H_2O(g) + CO_2(g)$, respectively.[30] In the present study, solvent in the ink is essential for the reduction of the NiO NP film. Indeed, the solvent-free NiO film that was dried at ambient condition for a long time or baked for rapid drying at a low enough temperature (~60 °C) failed to induce the reduction. We believe that in the case of using toluene as a solvent, protons are supplied from the toluene molecules adsorbed on the surfaces of the NiO NPs, and the laser irradiation initiates the reduction of NiO by the following reactions.

$$C_6H_5CH_3 \rightarrow C_6H_5CH_2^{-}(\text{toluene anion}) + H^+ \quad (1)$$

$$NiO + 2H^+ + 2e^- \rightarrow Ni + H_2O \quad (2)$$

Insufficient laser power cannot initiate the reaction of NiO with the reducing agents in the solvent. On the other hand, if the laser power exceeds the optimum level, the reduced electrodes undergo reoxidation and can be damaged or even destroyed at an extreme case. Therefore, it is postulated that the essentially competing phenomena of reduction and oxidation occur during the laser irradiation of the NiO NP ink-deposited films under ambient conditions. It is anticipated that the optimum laser process parameters lie in the regime where reduction dominates oxidation. Unveiling the exact mechanism of reduction of NiO film is the focus of ongoing study by the authors.

Recently, regular Ag grids have been developed as a new class of transparent conductor.[13,31] Likewise, regular Ni grids made with the method developed in this work can be applied as a transparent conductor. Figure 3a shows the effect of the grid pitch on substrate-based transmittance of the mesh electrodes on a glass substrate. By optimizing the pitch of the mesh patterns, we obtained patterned electrodes of high transmittance while maintaining low sheet resistance. The numbers on the patterns in Figure 3b indicate the pitch of each 1 cm × 1 cm mesh pattern. The picture was taken on printed letters as a background to illustrate the pattern transmittance. Figure 3c plots the sheet resistance and the corresponding transmittance at 550 nm wavelength as a function of the grid pitch. The sheet resistance was measured by the two-terminal methods while applying conductive silver paste at two sides of each area. As the pitch increases, the sheet resistance increases almost linearly while transmittance rises rapidly until the pitch reaches 80 μm. When the pitch is 80 μm, the mesh grids show transmittance of 87% while maintaining low resistance (655 Ω/sq). Although the sheet resistance is higher than the typical value of indium tin oxide (ITO), it is acceptable to low-current applications such as touch screen panels. As mentioned earlier, we verified that adjusting the concentration of the NiO ink and the spin speed during the thin film deposition procedures could produce thicker electrodes. Thus, thinner or thicker electrodes can be produced for suitable applications for higher transmittance and lower resistance, respectively. Figure 3d shows the resistivity data of the Ni electrodes as a function of laser power at a fixed 10 mm/s scan speed, which was calculated by $\rho = R \cdot (A/l)$, where *R*, *A*, and *l* are the resistance, the cross-sectional area, and the length of thin (average thickness = 38 nm) single line electrodes, respectively. The lowest resistivity under the optimized laser power (156−162 kW/cm^2 for glass substrates) is around 630 nΩ·m, which is about an order of magnitude higher than the resistivity of bulk nickel (ρ = 69.3 nΩ·m at room temperature), probably due to nanopores generated in the sintered electrode as

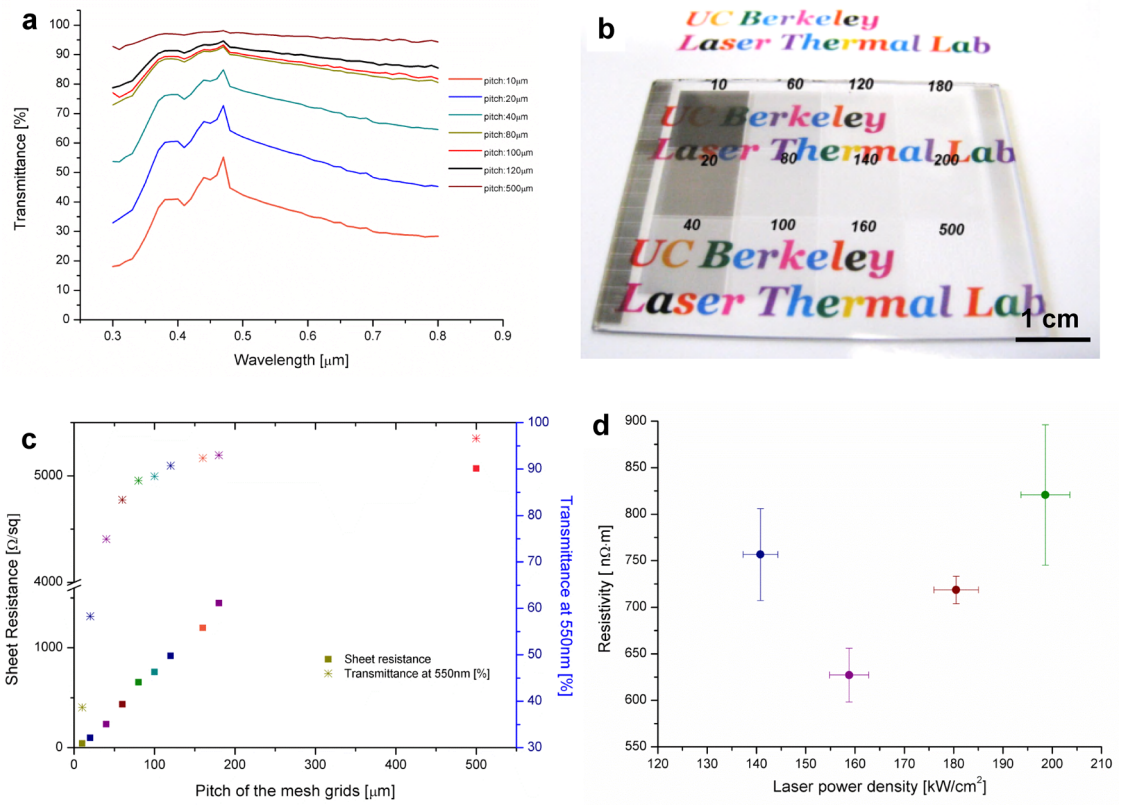

Figure 3. (a) Substrate-based transmittance data of the mesh-type electrodes on a glass substrate with different pitches. (b) Photoimage of several 1 cm × 1 cm mesh patterns. The number indicates the corresponding pitches of the mesh patterns. (c) Sheet resistance and the corresponding transmittance at 550 nm wavelength of each area shown in (b). (d) Resistivity data of the Ni electrodes (average thickness = 38 nm) as a function of laser power at the fixed 10 mm/s scanning speed. The resistivity of the bulk Ni is 69.3 nΩ·m.

noticed in Figure 2e, reoxidation, or incomplete reduction. However, the resistivity is still low enough to be used as high-resolution electrical conductors. For an adhesion test of the Ni electrode to a glass substrate, we performed the tape-pull test several times using a conventional adhesive tape (Magic tape, 3M) and verified that the Ni electrode did not detach from the substrate. Even after testing with a highly adhesive tape (single-sided adhesive copper tape, 3M), the electrodes on the substrate were intact and only adhesive residues remained on the surface, as displayed in Figure 4a. Moreover, the electrodes did not detach from the substrate even after dipping in an ultrasonic bath over 1 min. Since laser irradiation imparts a highly localized temperature field, it is a suitable tool for processing heat-sensitive flexible polymer substrates. Figure 4b shows mesh-type Ni electrodes on a polyimide (PI) substrate. The contrast of the area depends on the pitch of the mesh patterns as described above. The top and bottom insets show bright-field microscopic images of the mesh patterns of 20 and 80 μm pitch, respectively. The optimized laser power for reductive sintering on PI is around 42 kW/cm^2 with 10 mm/s scan speed when focused through a 10× objective lens, which is lower than that applied on a glass substrate. The lower power requirement on PI can be explained by recalling basics of transient diffusive heat transfer upon constant heat flux input. In this case, the induced temperature is proportional to the parameter $\alpha^{0.5}k^{-1}$, where α and k are the thermal diffusivity and conductivity, respectively.[32] As arranged in Table 1, the $\alpha^{0.5}k^{-1}$ value of PI is about 3 times higher than that of the soda-lime glass, in reasonable agreement with the ratio of the required laser powers for these substrates.

Figure 4c shows the cyclic bending test result of electrodes on a PI substrate. A 3.8 cm × 4.8 cm mesh-type pad was fabricated on the substrate, and copper tape was attached to the end of the two sides. Each side was then contacted to the copper blocks, one of which was attached to a motorized linear stage. As the copper block moves back and forth repeatedly, the pad is subject to continuous bending (bending radius = 0.4 cm). After over 5000 cycles, the measured resistance variation ($\Delta R/R_0$) is less than 6%. This superior bendability is attributed to the strong adhesion of the Ni electrodes to the PI substrate and also to the inherent resilience of ultrathin electrodes. Tape-pull and ultrasonic bath tests performed with PI substrate further confirmed strong adhesion of the electrodes on the PI substrate.

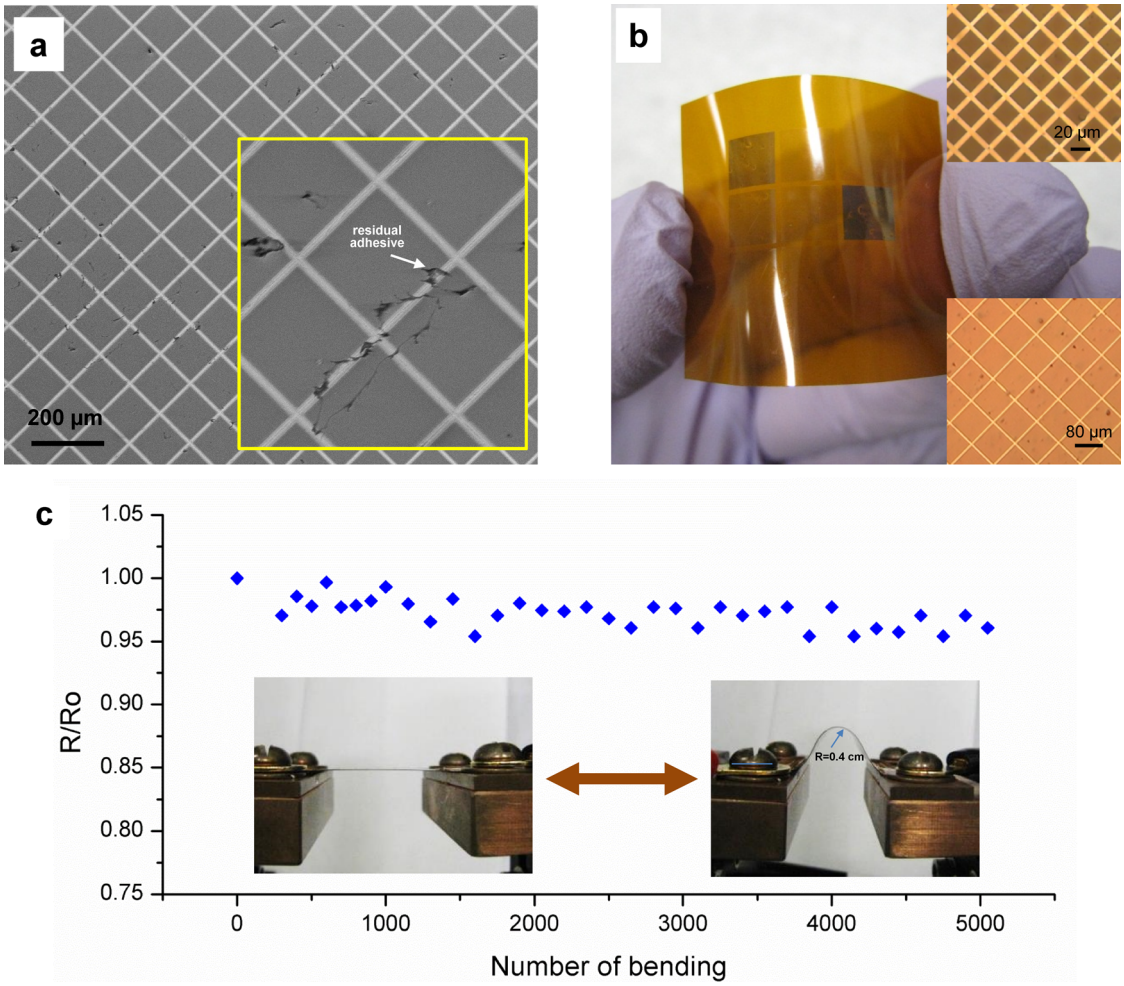

Figure 4. (a) SEM image of the mesh-type electrode after performing the tape-pull test several times with a highly adhesive tape. (b) Mesh-type Ni electrodes with different pitches on a polyimide substrate. The top and bottom insets show bright-field microscopic images of the mesh patterns of 20 and 80 μm pitches, respectively. (c) Measured resistance variation (R/R_0) after cyclic bending test with electrodes on a 3.8 cm $\times$ 4.8 cm polyimide substrate.

TABLE 1. Thermal Properties of Soda-Lime Glass and Polyimide Substrate

	thermal conductivity, k (W/mK)	thermal diffusivity, α (m^2/s)	$\alpha^{0.5}k^{-1}$
soda-lime glass[32]	1.4	9.1×10^{-7}	6.81×10^{-4}
polyimide (Kapton)	0.12	7.75×10^{-8}	2.32×10^{-3}

As a device demonstration, mesh-type Ni grids on a glass substrate were applied for a transparent 4-wire resistive touch screen panel, as shown in Figure 5a,b. A 3.8 cm $\times$ 4.8 cm mesh grid of 80 μm pitch was generated by the LDW process, and an ITO-PET film (60 Ω/sq, transmittance ~79% at 550 nm, Sigma-Aldrich) was used as a counter electrode. Two slips of copper tape were attached to the top and bottom sides of the ITO-PET film, with another two slips to the left and right sides of the Ni grids. The active area was 3 cm $\times$ 3.7 cm. A commercial USB-interface touch screen controller was connected to the four copper electrodes with electric wires through which the voltage was applied and converted the voltage drop signals into the letters on a PC screen. No protective coating layer was required for the Ni electrodes due to strong adhesion on the substrate. The performance of the Ni touch screen pad was evaluated as displayed in Figure 5c.

CONCLUSIONS

In summary, plastic-compatible maskless Ni electrode patterning was demonstrated by selective laser reductive sintering of air-stable NiO NP thin films deposited by a solution-processable route. All procedures, from materials synthesis to the laser processing, were performed under ambient conditions without involving photolithographic steps. Furthermore, the CW laser efficiently reduces and sinters the NiO NP film to a continuous Ni film in air through photothermal reaction of NiO with reducing agents in the solvent. Thin (~40 nm) Ni electrodes with fine morphology were produced due to the extremely small

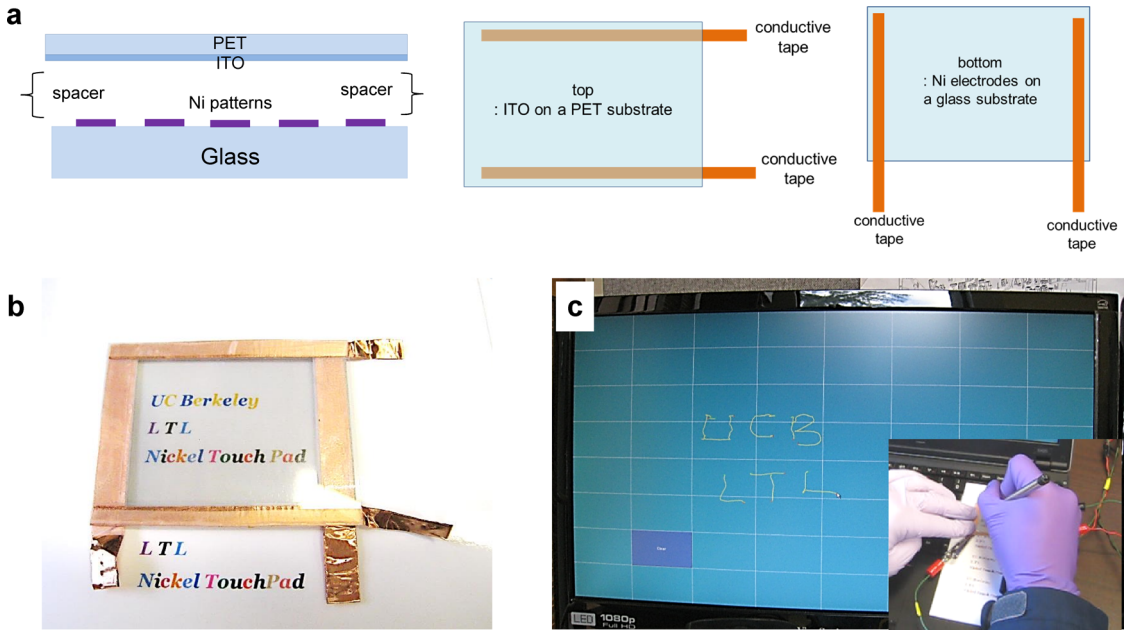

Figure 5. (a) Schematic diagram of a touch screen panel. (b) Photoimage of a 4-wire resistive touch screen panel. (c) Demonstration of operating Ni touch screen panel (active area = 3 cm × 3.7 cm) by writing "UCB LTL" with a stylus pen.

and uniform size of NiO NPs dispersed in the solvent without agglomeration. The resistivity of the Ni electrode is less than an order of magnitude higher compared to that of the bulk Ni. Cyclic bending, tape-pull, and ultrasonic bath tests confirm robust adhesion of the Ni electrodes on both plastic and glass substrates. Adjusting the pitch of the mesh-type thin electrode grids yields a transparent conductive panel showing a transmittance higher than 87% and a sheet resistance of around 655 Ω/sq. A resistive-type touch screen device employing a Ni mesh transparent conductor was demonstrated, showing steady performance without any protective layer over the electrodes.

Ni is hardy, rugged, and scratch-resistant. Moreover, Ni is abundant and inexpensive, compared to silver or ITO. Combined with low-cost solution processing, Ni printing can reduce the manufacturing cost of touch panels and other applications. Furthermore, Ni is highly resistant to corrosion. Printed Ni electrodes are therefore suitable in corrosive environments such as in batteries and electrochemical cells.

MATERIALS AND METHODS

NiO NP Ink Preparation. All chemicals were purchased from Sigma-Aldrich. Under ambient conditions, 0.257 g of nickel(II) acetylacetonate ($C_{10}H_{14}NiO_4$) and 0.32 mL of oleic acid ($C_{18}H_{34}O_2$) were dissolved in 15 mL of oleylamine ($C_{18}H_{37}N$) and heated to 110 °C with vigorous stirring. The solution was kept at 110 °C for more than 1 h to degas dissolved oxygen and evaporate moisture. The solution was cooled and kept at 90 °C, and then 0.339 mL of borane triethylamine complex ($(C_2H_5)_3N\cdot BH_3$) mixed with 2 mL of oleylamine was quickly injected into the solution. The resulting solution was kept at 90 °C for 1 h with vigorous stirring and cooled to room temperature. To collect the NiO NPs from the solution, 30 mL of ethanol (C_2H_6O) was added to the solution, and the mixture was then centrifuged at 3000−4000 rpm for 15 min. After the the residual solvents were removed, the nanoparticles were further washed with ethanol several times. The collected NPs were dispersed in toluene (C_7H_8) or α-terpineol ($C_{10}H_{18}O$) by sonication.

Conflict of Interest: The authors declare no competing financial interest.

Acknowledgment. Partial support to the Laser Thermal Laboratory by the King Abdullah University of Science and Technology (KAUST) is acknowledged. Laser Prismatics LLC was supported by the SBIR Phase I Grant No. 1346088 from the U.S. National Science Foundation. D.L. was supported by Gachon University research fund of 2014(GCU-2014-0107). The authors also would like to thank Dr. Frances I. Allen (Lawrence Berkeley National Lab) for assistance in recording TEM images.

REFERENCES AND NOTES

1. Shaheen, S. E.; Radspinner, R.; Peyghambarian, N.; Jabbour, G. E. Fabrication of Bulk Heterojunction Plastic Solar Cells by Screen Printing. *Appl. Phys. Lett.* **2001**, *79*, 2996–2998.
2. Pardo, D. A.; Jabbour, G. E.; Peyghambarian, N. Application of Screen Printing in the Fabrication of Organic Light-Emitting Devices. *Adv. Mater.* **2000**, *12*, 1249–1252.
3. Ko, S. H.; Chung, J.; Hotz, N.; Nam, K. H.; Grigoropoulos, C. P. Metal Nanoparticle Direct Inkjet Printing for Low-Temperature 3D Micro Metal Structure Fabrication. *J. Micromech. Microeng.* **2010**, *20*, 125010.
4. Ko, S. H.; Lee, D.; Hotz, N.; Yeo, J.; Hong, S.; Nam, K. H.; Grigoropoulos, C. P. Digital Selective Growth of ZnO Nanowire Arrays from Inkjet-Printed Nanoparticle Seeds on a Flexible Substrate. *Langmuir* **2011**, *28*, 4787–4792.
5. Secor, E. B.; Prabhumirashi, P. L.; Puntambekar, K.; Geier, M. L.; Hersam, M. C. Inkjet Printing of High Conductivity, Flexible Graphene Patterns. *J. Phys. Chem. Lett.* **2013**, *4*, 1347–1351.

6. In, J. B.; Lee, D.; Fornasiero, F.; Noy, A.; Grigoropoulos, C. P. Laser-Assisted Simultaneous Transfer and Patterning of Vertically Aligned Carbon Nanotube Arrays on Polymer Substrates for Flexible Devices. *ACS Nano* **2012**, *6*, 7858–7866.
7. Lee, D.; Pan, H.; Ko, S. H.; Park, H. K.; Kim, E.; Grigoropoulos, C. P. Non-vacuum, Single-Step Conductive Transparent ZnO Patterning by Ultra-short Pulsed Laser Annealing of Solution-Deposited Nanoparticles. *Appl. Phys. A: Mater. Sci. Process.* **2012**, *107*, 161–171.
8. Lee, D.; Pan, H.; Sherry, A.; Ko, S. H.; Lee, M.-T.; Kim, E.; Grigoropoulos, C. P. Large-Area Nanoimprinting on Various Substrates by Reconfigurable Maskless Laser Direct Writing. *Nanotechnology* **2012**, *23*, 344012.
9. Xiong, W.; Zhou, Y. S.; Hou, W. J.; Jiang, L. J.; Gao, Y.; Fan, L. S.; Jiang, L.; Silvain, J. F.; Lu, Y. F. Direct Writing of Graphene Patterns on Insulating Substrates under Ambient Conditions. *Sci. Rep.* **2014**, *4*, 4892.
10. Pan, H.; Lee, D.; Ko, S. H.; Grigoropoulos, C. P.; Park, H. K.; Hoult, T. Fiber Laser Annealing of Indium-Tin-Oxide Nanoparticles for Large Area Transparent Conductive Layers and Optical Film Characterization. *Appl. Phys. A: Mater. Sci. Process.* **2011**, *104*, 29–38.
11. Lee, M.-T.; Lee, D.; Sherry, A.; Grigoropoulos, C. P. Rapid Selective Metal Patterning on Polydimethylsiloxane (PDMS) Fabricated by Capillarity-Assisted Laser Direct Write. *J. Micromech. Microeng.* **2011**, *21*, 095018.
12. Son, Y.; Yeo, J.; Moon, H.; Lim, T. W.; Hong, S.; Nam, K. H.; Yoo, S.; Grigoropoulos, C. P.; Yang, D. Y.; Ko, S. H. Nanoscale Electronics: Digital Fabrication by Direct Femtosecond Laser Processing of Metal Nanoparticles. *Adv. Mater.* **2011**, *23*, 3176–3181.
13. Hong, S.; Yeo, J.; Kim, G.; Kim, D.; Lee, H.; Kwon, J.; Lee, H.; Lee, P.; Ko, S. H. Nonvacuum, Maskless Fabrication of a Flexible Metal Grid Transparent Conductor by Low-Temperature Selective Laser Sintering of Nanoparticle Ink. *ACS Nano* **2013**, *7*, 5024–5031.
14. Yeo, J.; Hong, S.; Lee, D.; Hotz, N.; Lee, M.-T.; Grigoropoulos, C. P.; Ko, S. H. Next Generation Non-vacuum, Maskless, Low Temperature Nanoparticle Ink Laser Digital Direct Metal Patterning for a Large Area Flexible Electronics. *PLoS One* **2012**, *7*, e42315.
15. Chung, J.; Bieri, N.; Ko, S.; Grigoropoulos, C.; Poulikakos, D. In-Tandem Deposition and Sintering of Printed Gold Nanoparticle Inks Induced by Continuous Gaussian Laser Irradiation. *Appl. Phys. A: Mater. Sci. Process.* **2004**, *79*, 1259–1261.
16. Chung, J.; Ko, S.; Bieri, N. R.; Grigoropoulos, C. P.; Poulikakos, D. Conductor Microstructures by Laser Curing of Printed Gold Nanoparticle Ink. *Appl. Phys. Lett.* **2004**, *84*, 801–803.
17. Kang, B.; Han, S.; Kim, J.; Ko, S.; Yang, M. One-Step Fabrication of Copper Electrode by Laser-Induced Direct Local Reduction and Agglomeration of Copper Oxide Nanoparticle. *J. Phys. Chem. C* **2011**, *115*, 23664–23670.
18. Joo, M.; Lee, B.; Jeong, S.; Lee, M. Laser Sintering of Cu Paste Film Printed on Polyimide Substrate. *Appl. Surf. Sci.* **2011**, *258*, 521–524.
19. Ryu, J.; Kim, H.-S.; Hahn, H. T. Reactive Sintering of Copper Nanoparticles Using Intense Pulsed Light for Printed Electronics. *J. Electron. Mater.* **2011**, *40*, 42–50.
20. Kim, H.-S.; Dhage, S. R.; Shim, D.-E.; Hahn, H. T. Intense Pulsed Light Sintering of Copper Nanoink for Printed Electronics. *Appl. Phys. A: Mater. Sci. Process.* **2009**, *97*, 791–798.
21. Nielsch, K.; Müller, F.; Li, A.-P.; Gösele, U. Uniform Nickel Deposition into Ordered Alumina Pores by Pulsed Electrodeposition. *Adv. Mater.* **2000**, *12*, 582–586.
22. Ahn, K.-S.; Nah, Y.-C.; Sung, Y.-E. Surface Morphological, Microstructural, and Electrochromic Properties of Short-Range Ordered and Crystalline Nickel Oxide Thin Films. *Appl. Surf. Sci.* **2002**, *199*, 259–269.
23. Knapp, J.; Follstaedt, D. Hall-Petch Relationship in Pulsed-Laser Deposited Nickel Films. *J. Mater. Res.* **2004**, *19*, 218–227.
24. Chae, J.; Park, H.-S.; Kang, S.-w. Atomic Layer Deposition of Nickel by the Reduction of Preformed Nickel Oxide. *Electrochem. Solid-State Lett.* **2002**, *5*, C64–C66.
25. Takano, N.; Hosoda, N.; Yamada, T.; Osaka, T. Mechanism of the Chemical Deposition of Nickel on Silicon Wafers in Aqueous Solution. *J. Electrochem. Soc.* **1999**, *146*, 1407–1411.
26. Slater, J. C. The Ferromagnetism of Nickel. *Phys. Rev.* **1936**, *49*, 537.
27. Park, S.-H.; Kim, H.-S. Flash Light Sintering of Nickel Nanoparticles for Printed Electronics. *Thin Solid Films* **2014**, *550*, 575–581.
28. Metin, Ö.; Özkar, S.; Sun, S. Monodisperse Nickel Nanoparticles Supported on SiO_2 as an Effective Catalyst for the Hydrolysis of Ammonia-Borane. *Nano Res.* **2010**, *3*, 676–684.
29. Soininen, P.; Elers, K.-E.; Saanila, V.; Kaipio, S.; Sajavaara, T.; Haukka, S. Reduction of Copper Oxide Film to Elemental Copper. *J. Electrochem. Soc.* **2005**, *152*, G122–G125.
30. Lister, T.; O'Driscoll, C.; Reed, N. *Classic Chemistry Demonstrations*; Royal Society of Chemistry: London, 1995; pp 132−135.
31. van de Groep, J.; Spinelli, P.; Polman, A. Transparent Conducting Silver Nanowire Networks. *Nano Lett.* **2012**, *12*, 3138–3144.
32. Incropera, F. P.; Lavine, A. S.; DeWitt, D. P. *Fundamentals of Heat and Mass Transfer*; John Wiley & Sons: New York, 2011; Chapter 5.